Available online at www.sciencedirect.com
SCIENCE DIRECT®
International Journal of Heat and Mass Transfer 47 (2004) 707–716
International Journal of HEAT and MASS TRANSFER
www.elsevier.com/locate/ijhmt

Computational simulation of a particle-laden RF inductively coupled plasma with seeded potassium

M. Shigeta, T. Sato, H. Nishiyama *

Institute of Fluid Science, Tohoku University, 2-1-1, Katahira, Aoba-ku, Sendai 980-8577, Japan

Received 28 February 2003; received in revised form 21 July 2003

Abstract

In the present study, the plasma properties, the thermofluid fields and the induction electromagnetic fields and further the in-flight particle behaviors in the radio frequency inductively coupled plasma (RF-ICP), which is electrically enhanced by seeding potassium vapor, are investigated by computational simulation. Since an electrically enhanced plasma is also influenced considerably by the applied coil frequency, the plasma structure and the in-flight particle behaviors in seeding potassium vapor are correspondingly influenced and have distinctive profiles. Due to the electrical enhancement of RF-ICP with potassium seeding, the frequency effect on particle heating becomes more considerable.

1. Introduction

Plasma is regarded as one of the multifunctional fluids [1] since it has high energy density, chemical reactivity, controllability by an external electromagnetic field and variable transport properties such as electrical conductivity. In the various kinds of plasma, a radio frequency inductively coupled plasma (RF-ICP) has advantages of large volume, clean high energy and chemical reactivity since it can be produced without electrodes. Furthermore, the chemical reaction time is comparatively long due to the low plasma velocity. It has, therefore, been extensively used in the reactive plasma spraying, synthesis of ultrafine powders and decomposition of hazardous substances such as freon and dioxin, for example. In these industrial applications, it is very important to control the plasma structure such as the plasma properties, the thermofluid fields and the induction electromagnetic fields and also the behaviors of the injected particles precisely [2–5].

It is well known that seeding a small amount of vaporized alkali metal with low ionization potential into plasma is one of the effective methods for the enhancement of the functions of plasma such as electrical conductivity [6,7]. When a small amount of alkali metal vapor is mixed to produce many electrons actively, the plasma controllability can be also enhanced by utilizing Lorentz force and Joule heating with increase in the electrical and thermal conductivities. There have, however, been a few papers clarifying the enhancement of the functions of RF-ICP by seeding alkali metal vapor [7,8]. No investigation into the effects of the functional enhancement on the behaviors of the in-flight particles in the plasma has never been conducted since a particle-laden RF-ICP with seeded alkali metal vapor is a complex interference system which is difficult for an experimental research.

In the present study, the plasma structure and the injected particle behaviors in the RF-ICP electrically enhanced by seeding potassium vapor are investigated by computational simulation in detail. The trajectory and the temperature evolution of an in-flight particle in the electrically enhanced plasma are obtained by a Lagrangian method. The particle phase change of melting and evaporation with the decrease in particle diameter are also taken into account. The effects of the applied coil frequency on the thermofluid of an electrically enhanced RF-ICP are investigated and the behaviors of the injected particle in the RF-ICP are also clarified. From these results, the important factor to control an RF-ICP is clarified.

* Corresponding author. Fax: +81-22-217-5261.
E-mail address: nishiyama@ifs.tohoku.ac.jp (H. Nishiyama).

0017-9310/$ - see front matter
doi:10.1016/j.ijheatmasstransfer.2003.08.007

Nomenclature

A	vector potential ($=(A_r, A_\theta, A_z)$), A H m^{-1}
a	thermal accommodation coefficient
c	specific heat of the particle, J kg^{-1} K^{-1}
C_D	drag force coefficient
C_p	specific heat at constant pressure, J kg^{-1} K^{-1}
D	diffusion coefficient, m^2 s^{-1}
D_{amb}	ambipolar diffusion coefficient, m^2 s^{-1}
d	diameter, m
e	electron charge, C
E	electric field ($=(E_r, E_\theta, E_z)$), V m^{-1}
f	frequency, Hz
F	Lorentz force ($=(F_r, F_\theta, F_z)$), N m^{-3}
h	enthalpy, J kg^{-1}
h_f	heat transfer coefficient, W m^{-2} K^{-1}
H	magnetic field ($=(H_r, H_\theta, H_z)$), A m^{-1}
Kn	Knudsen number
k	Boltzmann constant, J K^{-1}
k_{eq}	equilibrium constant, m^{-3}
k_{ion}	ionization coefficient, m^3 s
k_{re}	recombination coefficient, m^6 s^{-1}
L	latent heat, J kg^{-1}
m	mass, kg
n	number density, m^{-3}
P	coil input power, kW
p	pressure, Pa
Pr	Prandtl number
Q	flow rate, Sl min^{-1}
$\dot{Q}$	heat flux, J s^{-1}
$\overline{Q}$	mean collision cross-section, m^{-2}
Q_J	Joule heating, W m^{-3}
Q_r	radiation loss, W m^{-3}
Re	Reynolds number
r	radial coordinate, m
r_1	carrier gas nozzle radius, m
r_2	plasma gas nozzle radius, m
T	plasma temperature, K
T_a	ambient temperature, K
t	time, s
u	velocity component in axial direction, m s^{-1}
v	velocity component in radial direction, m s^{-1}
w	velocity component in azimuthal direction, m s^{-1}
x	mole fraction of liquid phase in a particle
z	axial coordinate, m

Greek symbols

δ	thickness, m
γ	specific heat ratio
η	viscosity, Pa s
θ	azimuthal coordinate, m
λ	thermal conductivity, W m^{-1} K^{-1}
μ_0	permeability in vacuum, H/m
ρ	density, kg m^{-3}
σ	electrical conductivity, S m^{-1}
ω	angular frequency, rad s^{-1}

Subscripts

Ar	argon atom
Ar^+	argon ion
K	potassium atom
K^+	potassium ion
e	electron
C	coil
W	wall
P	particle
f	film
s	surface
∞	bulk
m	melting
v	vaporizing
r	radial component
z	axial component
θ	azimuthal component

2. Numerical model

2.1. Plasma model

Fig. 1 shows a schematic illustration of the RF-ICP torch. The inlet portion has three nozzles for carrier gas, plasma gas and sheath gas respectively. An RF-ICP is produced and is maintained in the torch by the RF induction coils (0.5–13.56 MHz, 8 kW). The seed materials are prevaporized and injected into the plasma gas through the nozzle 2 as a premixed plasma gas.

The plasma model is proposed on the following assumptions [8]: steady, laminar and 2D axisymmetric flow and temperature fields; 2D axisymmetric induction electromagnetic fields with negligible displacement currents; negligible gravitational forces and viscous dissipation; local thermodynamic equilibrium (LTE) and optically thin; two-body collision ionization and three-body recombination; ambipolar diffusion of ions and electrons. There are some papers concerning the deviation of LTE especially under the low operating pressure or near wall in the coil region where the temperature gradient is steep in an RF-ICP [4,9,10]. The hypothesis of LTE or close-to-LTE is, however, considered to be valid for an RF-ICP operated at atmospheric pressure and at a coil frequency of a few MHz.

The governing equations of continuity, momentum, energy, and plasma species per unit volume are sum-

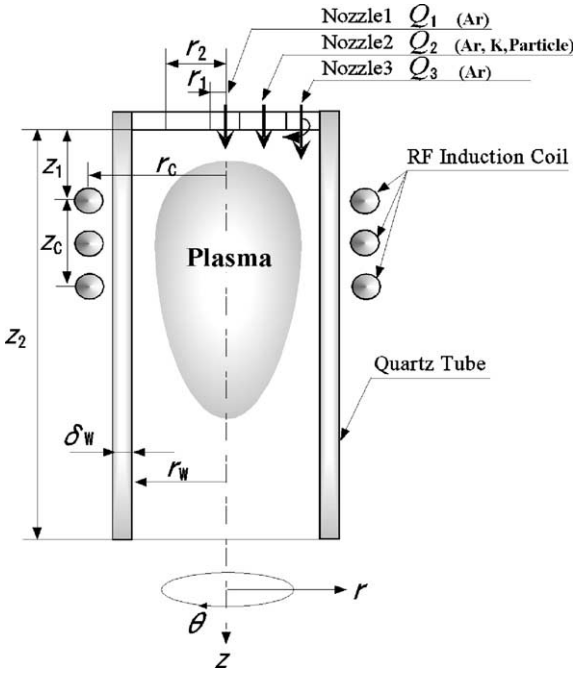

Fig. 1. Schematic illustration of a particle-laden RF-ICP torch with potassium seeding.

marized in the following general form in cylindrical coordinates:

$$\frac{\partial}{\partial z}(\psi u\phi)+\frac{1}{r}\frac{\partial}{\partial r}(r\psi v\phi) = \frac{\partial}{\partial z}\left(\Gamma\frac{\partial\phi}{\partial z}\right)+\frac{1}{r}\frac{\partial}{\partial r}\left(r\Gamma\frac{\partial\phi}{\partial r}\right)+S \quad (1)$$

where ϕ corresponds to physical variables such as u, v, w, h and n. ψ and Γ correspond to density and diffusion coefficient, respectively. In Eq. (1), the terms of the left hand side mean the convection, the first and second terms of the right hand side mean diffusion and the third term S represents the source term for each governing equation. Table 1 shows the transport variables and the source terms in the governing equations for the plasma flow. Since plasma is assumed to be electrically neutral, the electron number density is written as

$$n_e = n_{Ar^+} + n_{K^+}. \quad (2)$$

The governing equation of the induction electromagnetic fields is expressed as

$$\frac{\partial^2 A_\theta}{\partial z^2}+\frac{1}{r}\frac{\partial}{\partial r}\left(r\frac{\partial A_\theta}{\partial r}\right)-\frac{A_\theta}{r^2}=i\mu_0\sigma\omega A_\theta \quad (3)$$

where i is equal to $\sqrt{-1}$. The induction electromagnetic fields are represented using the electromagnetic vector potential for solving a 2D induction electromagnetic field equation to consider the interaction between the applied electromagnetic field of the coils and the induction electromagnetic field of the RF-ICP. For a standard induction plasma torch with the coil geometry as shown in Fig. 1, it is reasonable to assume that the electromagnetic field, and thus the vector potential, have only a azimuthal component. Then the induction electromagnetic fields are given by Maxwell's equations.

$$E_\theta = -i\omega A_\theta. \quad (4)$$

$$\mu_0 H_z = \frac{1}{r}\frac{\partial(rA_\theta)}{\partial r}. \quad (5)$$

$$\mu_0 H_r = -\frac{\partial A_\theta}{\partial z}. \quad (6)$$

The density, the specific heat at constant pressure and the radiation loss of the argon–potassium mixed plasma are replaced with those of the argon plasma since the seed fraction is very small in the present study [11,12]. The variation of the thermal conductivity caused by

Table 1
Transport variables and the source terms for the governing equations (1)

ϕ	ψ	Γ	S
1	ρ	0	0
u	ρ	η	$-\frac{\partial p}{\partial z}+\frac{\partial}{\partial z}\left(\eta\frac{\partial u}{\partial z}\right)+\frac{1}{r}\frac{\partial}{\partial r}\left(r\eta\frac{\partial v}{\partial z}\right)-\frac{2}{3}\frac{\partial}{\partial z}\left\{\eta\left[\frac{\partial u}{\partial z}+\frac{1}{r}\frac{\partial(rv)}{\partial r}\right]\right\}-\frac{1}{2}\mu_0\sigma\mathrm{Real}(E_\theta\overline{H}_r)$
v	ρ	η	$-\frac{\partial p}{\partial r}+\frac{\partial}{\partial z}\left(\eta\frac{\partial u}{\partial r}\right)+\frac{1}{r}\frac{\partial}{\partial r}\left(r\eta\frac{\partial v}{\partial r}\right)-\frac{2}{3}\frac{\partial}{\partial r}\left\{\eta\left[\frac{\partial u}{\partial z}+\frac{1}{r}\frac{\partial(rv)}{\partial r}\right]\right\}-\eta\frac{2v}{r^2}+\rho\frac{w^2}{r}+\frac{1}{2}\mu_0\sigma\mathrm{Real}(E_\theta\overline{H}_z)$
w	ρ	η	$-\frac{w}{r^2}\frac{\partial}{\partial r}(r\eta)-\rho\frac{vw}{r}$
h	ρ	λ/C_p	$\frac{1}{2}\sigma E_\theta\overline{E}_\theta-Q_r$
n_{Ar^+}	1	D_{Ar^+amb}	$k_{Ar\ ion}n_{Ar}n_e-k_{Ar\ re}n_{Ar^+}n_e$
n_{K^+}	1	D_{K^+amb}	$k_{K\ ion}n_K n_e-k_{K\ re}n_{K^+}n_e^2$
n_K	1	D_K	$k_{K\ re}n_{K^+}n_e^2-k_{K\ ion}n_K n_e$

Overbar (⁻) denotes the complex conjugate.

seeding is taken into account [13]. Since the electrical conductivity is expected to be remarkably enhanced with increase in electron number density by seeding a small amount of vaporized potassium, it is given as a function of electron number density.

$$\sigma = \frac{e^2 n_e}{m_e(c_e/l_e)} \tag{7}$$

where l_e and c_e are the mean free path and the mean value of the thermal velocity of electrons respectively.

Ambipolar diffusion coefficient of the heavy particle ion is given by

$$D_{h^+amb} = \frac{\mu_e D_{h^+} + \mu_{h^+} D_e}{\mu_e + \mu_{h^+}} \quad (h^+ = Ar^+, K^+) \tag{8}$$

where μ_e and μ_{h^+} are mobilities of electron and heavy particle ion respectively. On the other hand, diffusion coefficients of electron and heavy particle ion are given respectively by

$$D_e = \frac{kT_e}{m_e(c_e/l_e)} \tag{9}$$

$$D_{h^+} = \frac{kT}{m_{h^+}(c_{h^+}/l_{h^+})} \quad (h^+ = Ar^+, K^+) \tag{10}$$

where k, l_{h+} and c_{h+} are Boltzmann constant, the mean free path and the mean thermal velocity of heavy particle ions respectively. Collision cross-sections between each chemical species are used to calculate the mean free paths. They are given as functions of temperature from the experimental data [14,15] and especially Coulomb cross-section $\overline{Q}_{eh^+}$ is expressed

$$\overline{Q}_{eh^+} = 6\pi\left(\frac{e^2}{12\pi\varepsilon_0 kT_e}\right)^2 \ln\left\{\frac{9(4\pi\varepsilon_0 kT_e)^3}{4\pi n_e e^6}\right\}^{\frac{1}{2}} \quad (h^+ = Ar^+, K^+). \tag{11}$$

The recombination coefficients k_{re} of argon and potassium are taken from the available papers [16]. The ionization coefficient k_{ion} is expressed by

$$k_{ion} = k_{eq} \cdot k_{re} \tag{12}$$

where the equilibrium coefficient k_{eq} is estimated by Saha's equation under LTE and under the condition where no change in composition takes place.

As boundary conditions, non-slip condition, thermal conduction and electrical insulation are taken into account at the inner surface of the tube [8]. For the vector potential at the wall, the contributions from both the coil current and the induction current in the plasma are taken into account [17]. Since vector potential A_θ is complex, it is divided into the real part A_R and the imaginary part A_I in the present simulation. The inlet temperature T_{in} is set at 800 K so that the seed materials can be prevaporized before injection. T_w of 300 K is the outer-surface temperature of the tube.

A summary of the torch geometry and the operating conditions in the present calculation is given in Table 2, with reference to a commercial RF induction coupled plasma torch. The prevaporized potassium is injected from nozzle 2 as mixing with a plasma gas in seed fraction of 4.0% for example. The swirl flow ratio is given 5.0 at the nozzle 3 to stabilize the plasma. The inlet flow rates Q_1, Q_2 and Q_3 are 10.0, 10.0 and 25.0 Sl/min, respectively. The coil frequency f is chosen as 0.5 or 13.56 MHz without and with seeding respectively.

The governing equations for the velocity, temperature, concentration and electromagnetic fields, along with the boundary conditions, were solved using the SIMPLE algorithm developed by Patankar [18]. The computational simulation were performed for a 101 in r-direction by 101 in z-direction uniform staggered grid system.

2.2. Particle model

The particle behaviors injected into the plasma are simulated by simultaneous calculation of the particle trajectory and energy balance.

The particle model is proposed under the following assumptions: force acting on the particle is only drag force; spherical particle; no evaporation at temperatures lower than the boiling point; uniform temperature distribution in the particle due to low Biot number; no momentum and heat transfer from a particle to plasma in the dilute loading; variation of plasma transport properties by particle evaporation is neglected. The particle motion is described by

$$m_P \frac{d\mathbf{u}_P}{dt} = \frac{\pi}{8} d_P^2 \rho C_D (\mathbf{u} - \mathbf{u}_P)|\mathbf{u} - \mathbf{u}_P|. \tag{13}$$

Table 2
Torch geometry and operating conditions

Radius of nozzle1 r_1 (mm)	5.5
Radius of nozzle2 r_2 (mm)	17.0
Torch radius r_W (mm)	25.0
Coil radius r_C (mm)	33.0
Coil length z_C (mm)	20.0
Axial position of coil z_1 (mm)	30.0
Torch length z_2 (mm)	200.0
Wall thickness δ_W (mm)	5.0
Coil turn number N (turns)	3.0
Inlet temperature T_{in} (K)	800.0
Ambient temperature T_a (K)	300.0
Coil input power P (kW)	8.0
Coil frequency f (MHz)	0.5, 13.56
Operating pressure p (atm)	1.0
Injection flow rate Q_1, Q_2, Q_3 (Sl min^{-1})	10.0, 10.0, 25.0
Seed fraction SF (%)	4.0

From the viewpoint of multiphase flow dynamics, the added mass term and the Basset history term are significant under strongly non-steady conditions [19]. However, these terms can be neglected under the operating conditions in the present study due to the small size of the in-flight particle and the large density difference between the plasma and the particle [20].

The drag coefficient C_D is written as [21]

$$C_D = C_{Df} f_1 f_2 \tag{14}$$

$$C_{Df} = \begin{cases} \frac{24}{Re_{Pf}} & (Re_{Pf} < 0.2) \\ \frac{24}{Re_{Pf}}\left(1 + \frac{3}{16} Re_{Pf}\right) & (0.2 < Re_{Pf} < 2.0) \\ \frac{24}{Re_{Pf}}\left(1 + 0.11 Re_{Pf}^{0.81}\right) & (2.0 < Re_{Pf} < 21.0) \\ \frac{24}{Re_{Pf}}\left(1 + 0.189 Re_{Pf}^{0.62}\right) & (21.0 < Re_{Pf} < 200.0) \end{cases} \tag{15}$$

where particle Reynolds number Re_P is defined as

$$Re_P = \frac{d_P \rho}{\eta} |\mathbf{u} - \mathbf{u}_P|. \tag{16}$$

The film temperature is defined by

$$T_f = \frac{1}{2}(T_s + T_\infty). \tag{17}$$

Subscript f denotes film and the values are calculated on the film temperature for correction due to large temperature variation between the particle surface and plasma bulk [20].

The drag coefficient is corrected by the term f_1 expressing the variation of the transport properties in the particle boundary layer and the term f_2 expressing non-continuum effect for the small particle diameter.

$$f_1 = \left(\frac{\rho_\infty \eta_\infty}{\rho_s \eta_s}\right)^{-0.45} \tag{18}$$

$$f_2 = \left\{1 + \left(\frac{2-a}{a}\right)\left(\frac{\gamma}{1+\gamma}\right)\frac{4}{Pr_s} Kn\right\}^{-0.45} \quad (10^{-2} < Kn < 1) \tag{19}$$

where a is the thermal accommodation coefficient, γ the specific heat ratio, Kn the Knudsen number determined by the particle diameter and the effective mean free path length [20].

The particle temperature is obtained considering heat transfer by the plasma and radiation.

$$\dot{Q} = \pi d_P^2 [h_f (T - T_P) - \varepsilon_P \sigma_S (T_P^4 - T_a^4)] \tag{20}$$

For the phase change, $\dot{Q}$ is given by

$$\dot{Q} = \begin{cases} \frac{\pi}{6} \rho_P d_P^3 c \frac{dT_P}{dt} & (T_P < T_m, T_m < T_P < T_v) \\ \frac{\pi}{6} \rho_P d_P^3 L_m \frac{dx}{dt} & (T_P = T_m) \\ -\frac{\pi}{2} \rho_P d_P^2 L_v \frac{dd_P}{dt} & (T_P = T_v) \end{cases} \tag{21}$$

where T_m and T_v are melting point and boiling point, respectively.

The heat transfer coefficient h_f is written with Nusselt number.

$$h_f = \frac{\lambda_f}{d_p} Nu_f f_3 \tag{22}$$

$$Nu_f = (2 + 0.6 Re_{Pf}^{1/2} Pr_f^{1/3}) \left(\frac{\rho_\infty \eta_\infty}{\rho_s \eta_s}\right)^{0.6} \left(\frac{Cp_\infty}{Cp_s}\right)^{0.38} \tag{23}$$

This is also corrected by the term f_3 considering non-continuum effect due to the small particle diameter [22].

$$f_3 = \left\{1 + \left(\frac{2-a}{a}\right)\left(\frac{\gamma}{1+\gamma}\right)\frac{4}{Pr_s} Kn\right\}^{-1} \quad (10^{-3} < Kn < 1) \tag{24}$$

Especially for the investigation into the effects of the functionally enhanced RF-ICP on the in-flight particle behavior injected with plasma gas from Nozzle 2, the particle injected from the radial position of 11.25 mm is particularly focused as a representative. The initial temperature and initial diameter of an injected particle are given as 300 K and 20 μm, respectively. The initial velocity of the particle is assumed 70% of the carrier gas velocity at the position [23].

3. Results and discussion

The distributions of the plasma properties and the thermofluid fields in the RF-ICP and further the particle behaviors are investigated by computational simulation for four cases in Table 3. In the present paper, the control parameters are the seed material and the coil frequencies. The particle material are copper, nickel and tungsten and the data of their properties are given for the realistic numerical simulation [24].

3.1. Plasma properties and thermofluid fields in the RF-ICP

Fig. 2(a) and (b) show the electron number density distributions in Cases 1–4. In seeding a small amount of potassium (4.0%), the electrons exist much wider and the maximum values increase near the coil since potassium ionizes easily with much lower ionization potential than Argon regardless of the applied coil frequency. When the applied frequency is 13.56 MHz, the distributions

Table 3
Controlled variables

	Seed material	Coil frequency f (MHz)
Case1	Without seed	0.5
Case2	K	0.5
Case3	Without seed	13.56
Case4	K	13.56

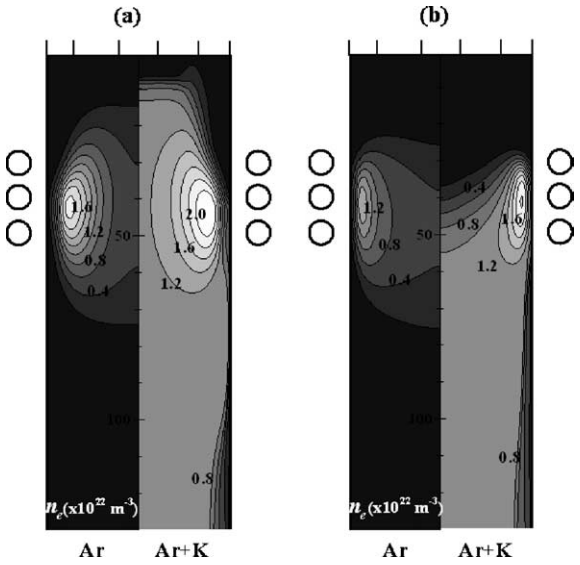

Fig. 2. Electron number density distributions: (a) $f = 0.5$ MHz and (b) $f = 13.56$ MHz.

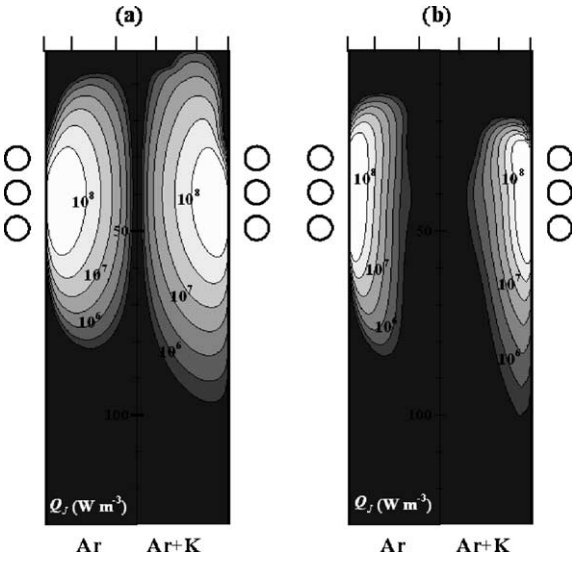

Fig. 4. Joule heating distributions: (a) $f = 0.5$ MHz and (b) $f = 13.56$ MHz.

approach nearer to the wall along with the temperature distributions as stated later.

Fig. 3(a) and (b) show the electrical conductivity distributions in Cases 1–4. The high electrical conductivity regions extend axially with the considerable increase in electron number density by potassium seeding for both coil frequencies. This phenomenon means that the plasma is electrically enhanced by seeding potassium, which also results in the enhancement of the controllability of the plasma by external electromagnetic fields.

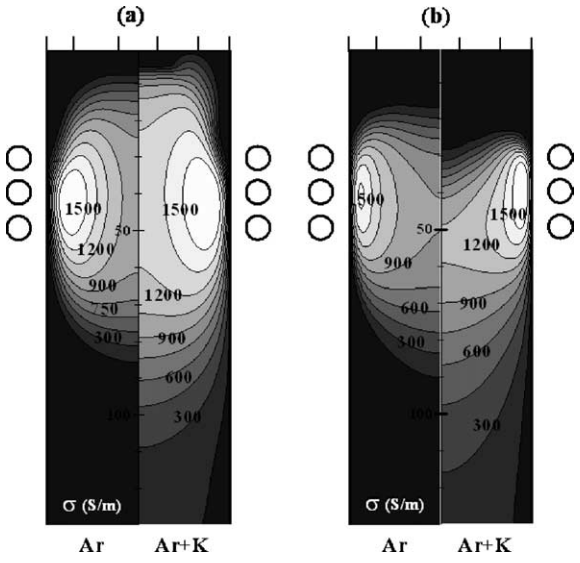

Fig. 3. Electrical conductivity distributions: (a) $f = 0.5$ MHz and (b) $f = 13.56$ MHz.

Fig. 4(a) and (b) show the Joule heating distributions calculated by $\sigma E_\theta \overline{E}_\theta/2$ in Cases 1–4. They extend longer and have the same tendencies as the electrical conductivity distributions as shown in Fig. 3. When the applied coil frequency is 13.56 MHz, the Joule heating concentrates nearer to the wall due to the skin effect which is closely related to skin depth $\delta = (2\pi\mu_0\sigma f)^{-\frac{1}{2}}$. The higher the applied coil frequency is, the smaller the skin depth becomes. With potassium seeding, the Joule heating concentrates nearer to the wall since the electrical conductivity is higher there as shown in Fig. 3.

Fig. 5(a) and (b) show the plasma temperature fields in Cases 1–4. In the cases of $f = 0.5$ MHz, the high temperature region becomes wider by potassium seeding along with the Joule heating which is the heat source of the RF-ICP. On the other hand, the distribution shortens axially with potassium seeding due to the wall concentration of the Joule heating in the cases of $f = 13.56$ MHz. Comparing the cases between potassium seeding and no seeding, the variations of especially the high temperature regions by the applied coil frequencies are more remarkable in seeding potassium. This means that potassium seeding enhances the controllability of the temperature field of the RF-ICP by the applied coil frequency.

Fig. 6(a) and (b) show the plasma velocity fields in Cases 1–4. By seeding potassium, the velocity fields change for both frequencies. But the difference by seeding potassium is small because of the cancellation effect, since the increase in the viscous force effect in the high temperature field and Lorentz forces in the potassium seeded RF-ICP interfere complexly. The difference of the velocity fields between $f = 0.5$ and 13.56 MHz is

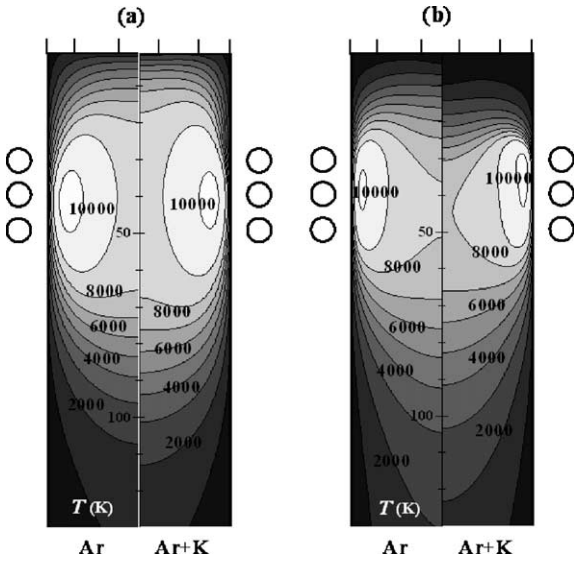

Fig. 5. Plasma temperature fields: (a) $f = 0.5$ MHz and (b) $f = 13.56$ MHz.

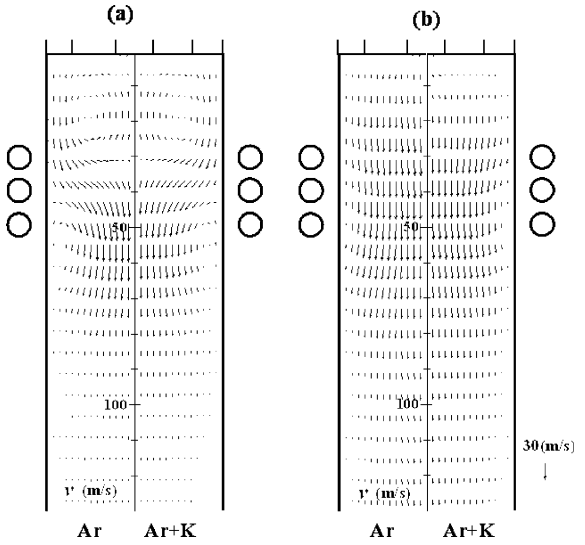

Fig. 6. Plasma velocity fields: (a) $f = 0.5$ MHz and (b) $f = 13.56$ MHz.

quite remarkable regardless of potassium seeding. When the applied coil frequency is 0.5 MHz, a recirculating flow exists in the upstream region of the torch because the flow is strongly pinched by the radial Lorentz force in the RF-ICP. On the other hand, the flow is almost straight in the cases of $f = 13.56$ MHz. This is because the Lorentz forces concentrate near the wall due to skin effect with the high coil frequency, which is the same tendency as the Joule heating as shown in Fig. 4. The absolute values of Lorentz force, however, are smaller than the cases of $f = 0.5$ MHz since the coil currents may decrease as the coil frequency increases.

3.2. Particle behaviors

Fig. 7 show the particle trajectories for a copper particle as a representative. In the cases of $f = 0.5$ MHz, a particle approaches slightly to the wall in the upstream region of the torch and then return to the axis of the torch because of the recirculating flow as shown in Fig. 6. In the cases of $f = 13.56$ MHz, the injected particle travels straight due to the absence of the recirculating flow in the plasma. However, the difference of the trajectories is small with or without potassium seeding.

Fig. 8 show the particle axial velocity evolution for copper as a representative. In the cases of $f = 0.5$ MHz, the particle axial velocities decrease in the upstream region of the torch due to the recirculating flow as shown in Fig. 6 and then drastically increase just downstream of the coil region. The particle is axially accelerated simply in the cases of $f = 13.56$ MHz. The effect of potassium seeding on the particle axial velocity is not very remarkable.

Fig. 9(a) and (b) show the particle temperature evolution for Cases 1–4. The temperatures of all the particles increase drastically, reach their boiling points and start to evaporate in the upstream region of the torch. In any cases, copper and nickel have similar profiles but tungsten shows more rapid increase due to the lower heat capacity. When the applied coil frequency is 0.5 MHz, the particles obtain more heat from plasma according to the extension of the high temperature region as shown in Fig. 5 regardless of potassium seeding. With potassium seeding in Fig. 9(b), the effect of applied frequency on particle heating is more remarkable than

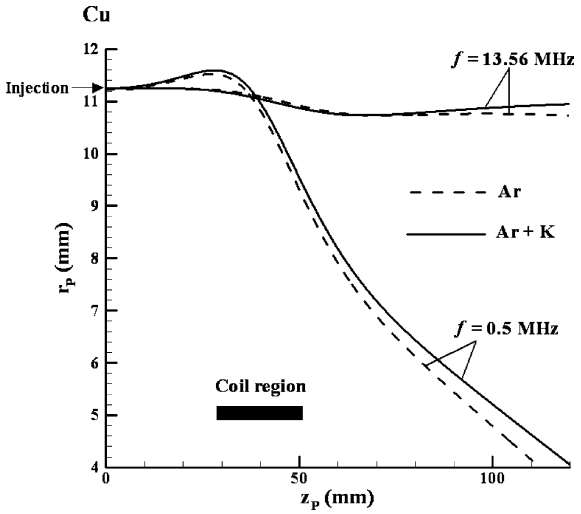

Fig. 7. Particle trajectories for copper.

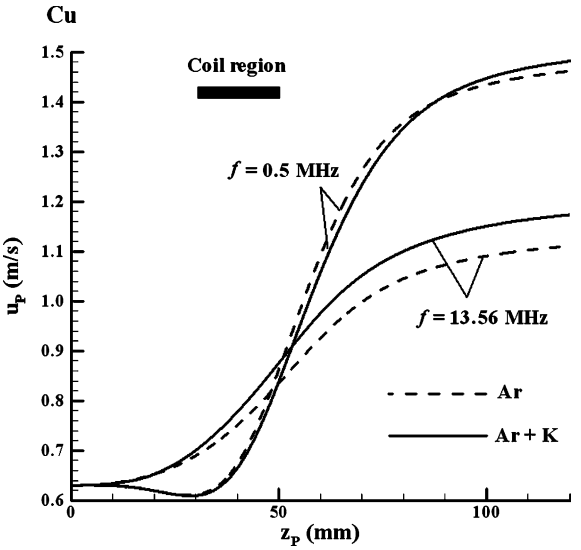

Fig. 8. Particle axial velocity evolution for copper.

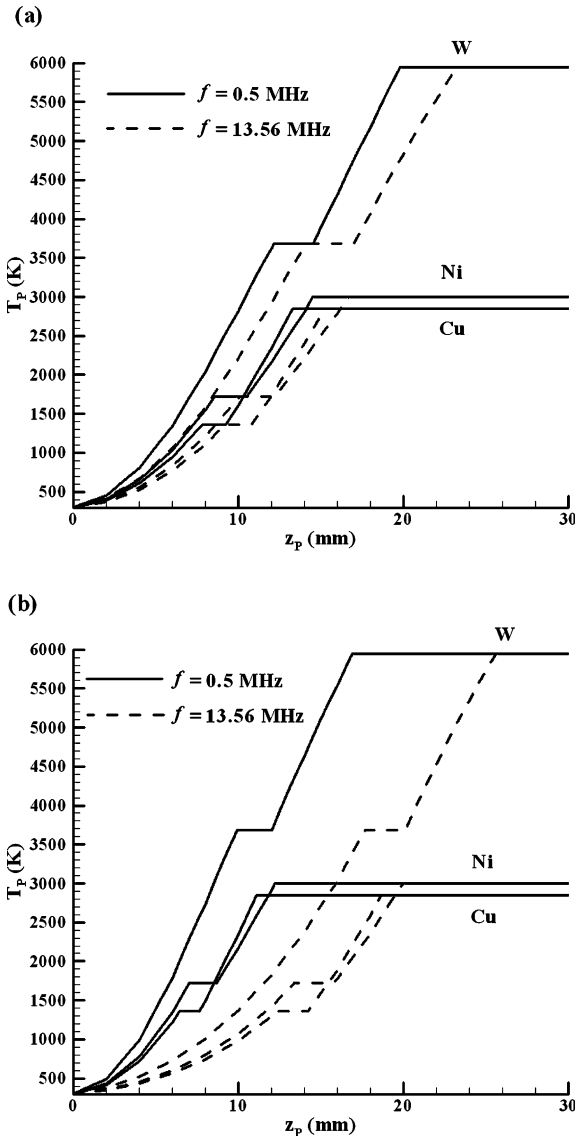

Fig. 9. Particle temperature evolution (a) Ar and (b) Ar+K.

the case without seeding in Fig. 9(a). Focusing on the axial starting points of evaporation of tungsten as an example, they are $z_P = 19.8$ and 23.2 mm without potassium seeding, while $z_P = 16.9$ and 25.6 mm with potassium seeding in $f = 0.5$ and 13.56 MHz respectively. This means that it is possible to adjust the particle heating by the applied coil frequency easily with potassium seeding.

Fig. 10(a)–(c) show the particle diameter evolution with evaporation in Cases 1–4 for each material of particles. The particle diameters decrease with evaporation and then reach the constant values finishing evaporation. In any cases, the lower the applied coil frequency is, the smaller the final particle diameters become. With potassium seeding, the final particle diameters show smaller in $f = 0.5$ MHz because of the active evaporation, while those show larger in $f = 13.56$ MHz. To investigate the effect of potassium seeding on the variable range of the particle diameter, the values of the final particle diameter difference Δd_P between in $f = 0.5$ and 13.56 MHz divided by the initial particle diameter $d_{P0} = 20$ μm for each case are shown in Table 4. With potassium seeding, the values for each material show from 1.6 to 1.9 times as large as those without seeding, which means that the controllable range of evaporated diameter by the applied frequency becomes larger.

4. Conclusions

The plasma structure and the in-flight particle behaviors in the RF-ICP electrically enhanced by seeding potassium vapor are investigated and the effects of the applied coil frequency as an important factor to control an RF-ICP are also clarified by computational simulation.

1. By seeding a small amount of potassium, the high electrical conductivity regions extend along with the increase in electron number density since potassium ionizes with much lower ionization potential than Argon. Correspondingly, Joule heating distributions also extend longer. The high temperature region also changes by potassium seeding depending on the applied coil frequency. These distributions concentrate near the wall due to the skin effect in the cases of

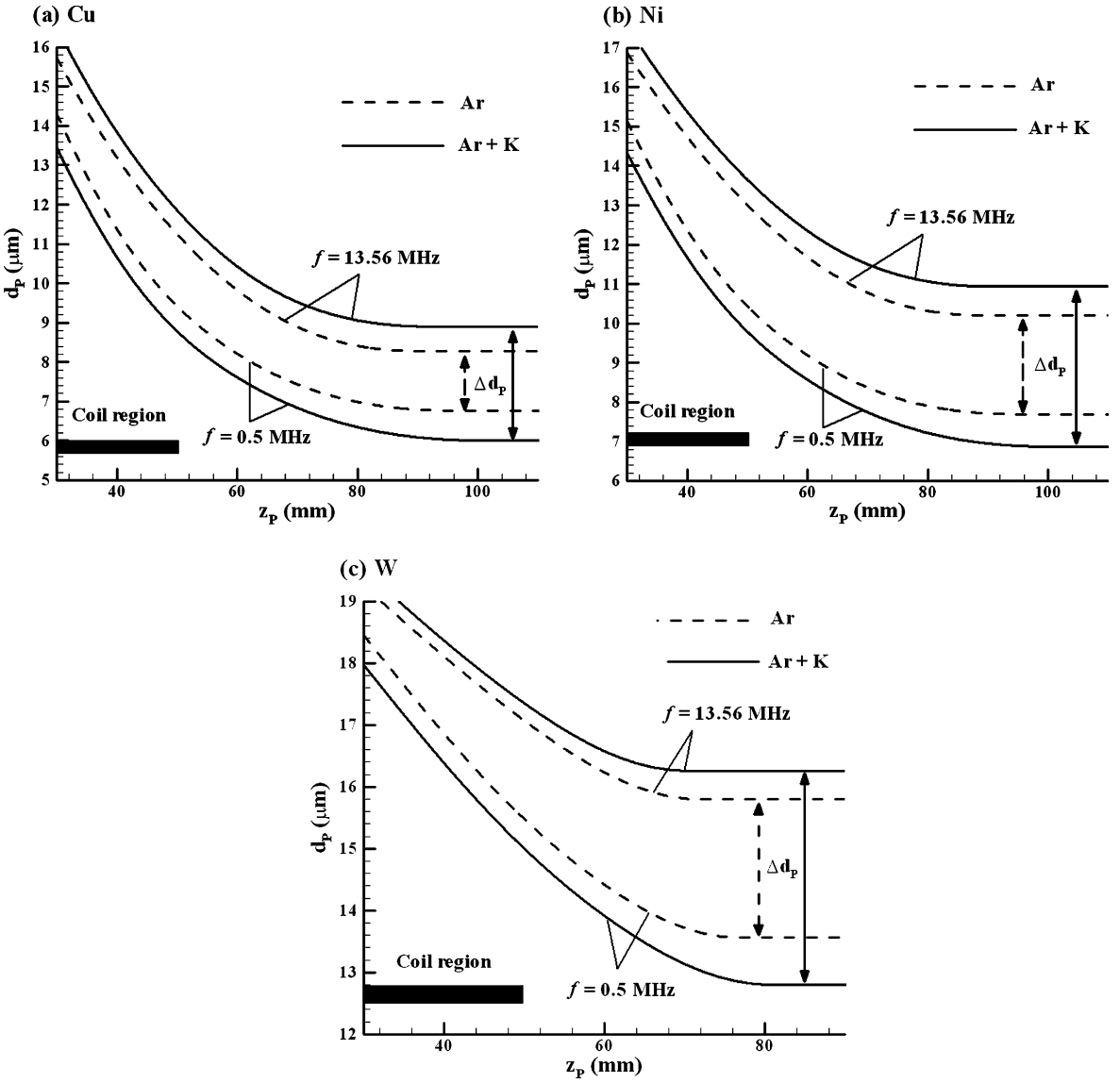

Fig. 10. Particle diameter evolution with evaporation: (a) copper, (b) nickel and (c) tungsten.

Table 4
Seeding effect on the variable range by the applied coil frequency

	$(\Delta d_P/d_{P0}) \times 100$ (%)	
	(Ar)	(Ar+K)
Cu	7.5	14.5
Ni	12.5	20.5
W	11.0	17.5

$f = 13.56$ MHz. The variations of the high temperature regions by the applied coil frequencies are more remarkable with seeding potassium than without seeding. In the plasma velocity fields, a recirculating flow exists in the upstream region for low applied frequency due to the pinch effect when the applied coil frequency is 0.5 MHz. But there is small seeding effect on velocity field structure.

2. The trajectories and the axial velocity evolution of the in-flight copper particles are different for each case along with the difference of the plasma velocity fields depending on the applied coil frequency. The effect of the applied coil frequency is more dominant than that of the potassium seeding. The temperature of the particle increases drastically, reaches their boiling points and starts to evaporate in the upstream region of the torch. With potassium seeding, the

differences of the profiles are more remarkable and the profiles shift upstream considerably with the lower frequency compared with the case without seeding. The final particle diameter shows smaller with the lower applied coil frequency. The difference of the final particle diameter by the applied coil frequency is larger with potassium seeding, which means that the controllable range of the processed particle diameter by the applied frequency becomes larger.

Acknowledgements

This work was partly supported by a grant-in-aid for Scientific Research (B) from the Japan Society for Promotion Science (2001, 2002). This computational simulation was conducted under the collaboration research project (2002) using an Origin 2000 at the Advanced Fluid Information Research Center of the Institute of Fluid Science, Tohoku University, Japan.

References

[1] Japan Society of Mechanical Engineers, Functional fluids and intelligent fluids, Corona Publishing Corporation, Japan, 2000 (in Japanese).
[2] J.H. Park, S.H. Hong, Numerical analysis of nitrogen-mixed argon plasma characteristics and injected particle behavior in an ICP torch for ultrafine powder synthesis, IEEE Trans. Plasma Sci. 23 (1995) 532–538.
[3] H. Nishiyama, Y. Muro, S. Kamiyama, The control of gas temperature and velocity fields of a RF induction thermal plasma by injecting secondary gas, J. Phys. D: Appl. Phys. 29 (1996) 2634–2643.
[4] H. Nishiyama, N. Fukai, S. Kamiyama, Functionalization of a nonequilibrium RF induction plasma by gas mixtures, JSME Int. J. Ser. B. 41 (1998) 502–510.
[5] R.J. Rosa, Magnetohydrodynamic Energy Conversion Rev., Hemisphere, New York, 1987.
[6] H. Nishiyama, T. Sato, A. Veefkind, S. Kamiyama, Functional enhancement of a non-equilibrium plasma jet by seeding in the applied magnetic field, Heat Mass Transfer 30 (1995) 291–296.
[7] T. Suekane, T. Taya, Y. Okuno, S. Kabashima, Numerical studies on the nonequilibrium inductively coupled plasma with metal vapor ionization, IEEE Trans. Plasma Sci. 24 (1996) 1147–1154.
[8] H. Nishiyama, M. Shigeta, Numerical simulation of an RF inductively coupled plasma for functional enhancement by seeding vaporized alkali metal, Eur. Phys. J., Appl. Phys. 18 (2002) 125–133.
[9] J. Mostaghimi, P. Proulx, M.I. Boulos, A two-temperature model of the inductively coupled plasma, J. Appl. Phys. 61 (5) (1987) 1753–1760.
[10] D.V. Gravelle, M. Beaulieu, M.I. Boulos, A. Gleizes, An analysis of LTE effects in inductively coupled RF plasmas, J. Phys. D: Appl. 22 (1989) 1471–1477.
[11] J. Menart, H. Lin, Numerical study of high-intensity free-burning arc, J. Thermophys. Heat Transfer 12 (1998) 500–506.
[12] M.I. Boulos, P. Fauchais, E. Pfender, in: Thermal Plasma, vol. 1, Plenum Press, New York, 1994.
[13] L.E. Kalikhman, Elements of Magnetogasdynamics, Saunders, Philadelphia, 1967.
[14] J. Kanzawa, Plasma Heat Transfer, Shinzan Corporation, Japan, 1992.
[15] F.E. Spencer, A.V. Phelps, Momentum transfer cross-section and conductivity integrals for gases of MHD interest, in: 15th Symposium Engineering Aspects of MHD IX, 1976, pp. 9.1–9.12.
[16] The 153rd Committee on Plasma Materials Science, Japan Society for the Promotion of Science, Plasma Materials Science Handbook, Ohm Corporation, Japan, 1992.
[17] J. Mostaghimi, M.I. Boulos, Two-dimensional electromagnetic field effects in induction plasma modeling, Plasma Chem. Plasma Process. 9 (1989) 25–44.
[18] S.V. Patankar, Numerical Fluid Flow and Heat Transfer, Hemisphere, New York, 1980.
[19] S. Kawano, H. Hashimoto, T. Suyama, Buoyancy-driven accelerated motion of an encapsulated liquid drop, JSME Int. J. B 37 (1) (1994) 30–37.
[20] E. Pfender, Y.C. Lee, Particle dynamics and particle heat and mass transfer in thermal plasmas. Part I: The motion of a single particle without thermal effects, Plasma Chem. Plasma Proc. 5 (3) (1985) 211–237.
[21] M.I. Boulos, Heating of powders in the fire ball of an induction plasma, IEEE Trans. Plasma Sci. PS-6 (2) (1978) 93–106.
[22] Y.C. Lee, Y.P. Chyou, E. Pfender, Particle dynamics and particle heat and mass transfer in thermal plasmas. Part II: particle heat and mass transfer in thermal plasmas, Plasma Chem. Plasma Proc. 5 (4) (1985) 391–414.
[23] Y. Tsuji, Basis of Pneumatic Transport, Youkendo Publishing, Japan, 1984.
[24] O.P. Solonenko, A.V. Smirnov, V.A. Klimenov, V.G. Butov, Y.F. Ivanov, Role of interfaces in splat and coatings structure formation, Phys. Mesomech. 2 (1–2) (1999) 113–129.